Blind Source Separation – Based Motion Detector for Sub-Micrometer, Periodic Displacement in Ultrasonic Imaging

Md Murad Hossain[1], Diwash Thapa[2], Justin Sierchio[2], Amy Oldenburg[2], Caterina Gallippi1[1]
[1]Joint Department of Biomedical Engineering, University of North Carolina, Chapel hill, North Carolina, USA,
[2]Department of Physics and Astronomy, University of North Carolina, Chapel hill, North Carolina, USA,

***Abstract*— Sub-micrometer, periodic motion detection using blind source separation (BSS) via principal component analysis (PCA) is presented in the context of magnetomotive ultrasound (MMUS) imaging and Shearwave Dispersion Ultrasound Vibrometry (SDUV). In MMUS, an oscillating external magnetic field displaces tissue loaded with superparamagnetic iron oxide (SPIO) particles, whereas in SDUV, periodic tissue motion is induced using acoustic radiation force (ARF) to measure visco-elastic properties. BSS motion detection performance in MMUS imaging and SDUV was compared against frequency-phase locked (FPL) and normalized cross-correlation (NCC) motion detectors, respectively, *in silico* and in experimental phantoms. Parametric MMUS phantom images constructed using the BSS method had nearly twice the SNR of the corresponding images constructed using FPL method when a 0.043 mm or smaller kernel size was used. In FEM models of SDUV, the error in the BSS-estimated viscoelastic properties of simulated materials was < 10%, whereas the error was > 20% using NCC when the simulated SNR was 15 dB. In a calibrated elasticity phantom, the amplitude of the motion was ≤ 0.5 µm for a scanner power level ≤ 20%. The median percent error in BSS-derived shear modulus of the phantom was -6.8%, -1.55%, -17.11% for power level of 20%, 15%, and 10%, respectively. The corresponding NCC-derived errors were 29.90%, 127.1%, and 244.70%. These results suggest the relevance of using BSS for the detection of sub-micrometer, periodic motion in MMUS and SDUV imaging, particularly when SNR is less than 15 dB and/or induced displacements are less than 0.5 µm.**

Keywords— Blind Source Separation (BSS); Motion Detection; MMUS Imaging; SDUV

I. Introduction

Detecting motion in tissue has diagnostic relevance, and applications based on ultrasound-derived motion information have been developed due to its low-cost, real-time imaging capabilities, ease-of-use, and ability to non-invasively characterize motion within the human body. In magnetomotive ultrasound (MMUS) [1], an oscillating external magnetic field displaces tissue loaded with superparamagnetic iron oxide (SPIO) particles, whereas in Shearwave Dispersion Ultrasound Vibrometry (SDUV) [2], [3] and Harmonic Motion Imaging (HMI)[4], [5], periodic motion is induced using ARF to measure the viscoelastic properties of tissue. Frequency- and phase-locked (FPL) [1], Kalman filtering [7], and normalized cross-correlation (NCC) [6] methods have been used to detect motion in MMUS, SDUV, and HMI, respectively. In MMUS, parametric images of the detected motion magnitude at the oscillation frequency and phase are rendered. In SDUV and HMI, detected motion is used to measure viscoelastic properties of tissue as a point measurement. For all three techniques, overall performance is impacted by error in the motion estimation arising from electronic noise, signal decorrelation, finite tracking-lengths, bandwidth, and sampling-rates. The effect of these parameters on estimator performance is given by the Cramer-Rao Lower Bound (CRLB), which places a bound on the minimum estimation error variance that can be achieved in a specific, imaging situation by an unbiased estimator [10]. For most commercially available ultrasound scanners, induced motion must be roughly 0.6 µm to overcome the CRLB and enable detection using NCC. We herein implement BSS to enable detection of motion smaller than this limit.

To improve the quality of MMUS image, data are collected by turning on and off the magnetic field modulation, and then, ′magnetic field off′ data is subtracted from the ′on′ data to remove ambient noise. However, this does not remove motion artifacts if noise and the oscillating magnetic field have overlapping spectra. Conventional frequency domain filtering methods are not necessarily effective for separating signal from noise in ultrasonic applications involving short data lengths or signal components with overlapping frequency spectra. Regression filters [11] offer an alternative to frequency domain approaches for signal separation. Adaptive regression filtering can be accomplished by blind source separation (BSS). BSS via principal component analysis (PCA) has been used for clutter rejection, physiological motion filtering, and radiation force induced displacement filtering [12]–[15].

In this work, we investigate the feasibility of using BSS for detecting sub-micrometer, periodic motion in the context of MMUS imaging and SDUV. The proposed methods are evaluated in finite-element method (FEM) models and tissue mimicking phantoms, and the results are compared against FPL and NCC methods for detecting motion in MMUS imaging and SDUV, respectively.

II. BackGround

BSS is a method for recovering unobserved signals or "sources" from several realizations of their mixture based on assumed statistical relationships between the sources [16]. PCA assumes that the source signals are orthogonal and Gaussian-distributed. It can be performed by the Karhunen–Loeve (KL) transform to decompose the input data matrix into its orthogonal basis functions with a corresponding energetic signature. Steps for performing motion detection using BSS via PCA for MMUS and SDUV are shown in Figure 1. Note that for step 3, BSS is applied to translating axial kernels. Note that an image will be formed at the final step for MMUS imaging, whereas a point measure of viscoelastic properties will be given for SDUV.

This work was supported by NIH grants R01DK107740, R01NS074057, and K02HL105659.

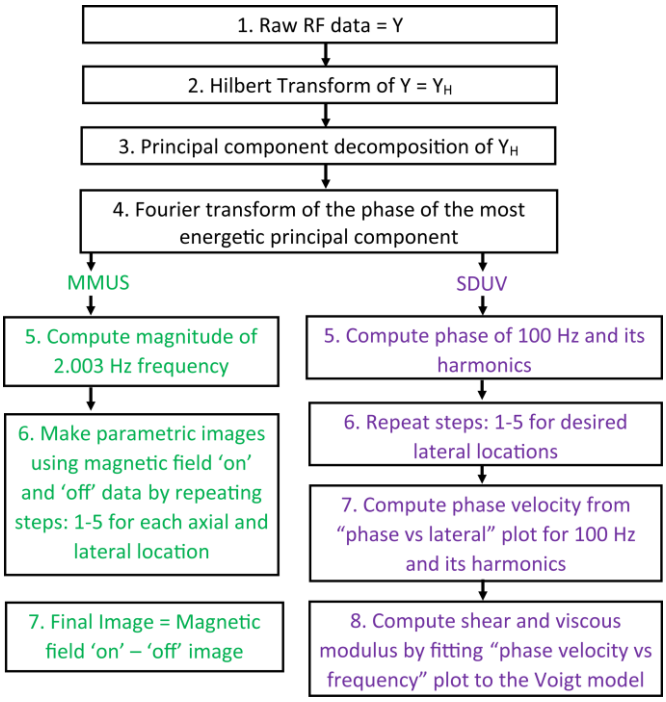

Figure 1: Steps for processing MMUS and SDUV data using the BSS method. Common steps are shown in black text color; different processing steps are shown in green (MMUS) and purple (SDUV) text.

III. Materials and Methods

A. Filed II Simulation of Periodic Motion Detection

An idealistic, three-dimensional, simulated phantom, containing stationary and nonstationary ultrasonic scatterers, was created in Field II [17], [18]. Table 1 (2nd column) describes the relevant simulation parameters. The simulated phantom spanned from 17.5 to 32.5 mm axially, -5 to 5 mm laterally, and -2.5 to 2.5 mm elevationally, with 10 scatterers randomly distributed per resolution cell. Scatterers positioned from 23 to 27 mm axially, -2 to 2 mm laterally, and -2 to 2 mm elevationally underwent sinusoidal motion at 2 Hz with amplitude 0.5 μm. Outside this volume, scatterers were stationary. The scattering magnitude of both moving and stationary scatterers followed a Gaussian distribution with mean 0 and standard deviation 10. Simulated RF data by Field II were processed using our BSS method (Figure 1) with a 0.1λ kernel to construct a parametric MMUS-type image.

B. FEM Simulations of SDUV

The FEM model developed by Palmeri *et al.* [19] was used to simulate the dynamic responses of a viscoelastic solid to a 3D impulsive ARF excitation utilizing LS-DYNA3D (Livermore Software Technology corp. Livermore, CA). A three-dimensional, rectangular, solid mesh with dimension 25x17x8 mm (axial x lateral x elevation) was assembled from 0.2 mm, cubic elements using LS- PREPOST (Livermore Software Technology Corp., Livermore, CA). To reduce computational time, quarter-symmetry was assumed in both the lateral and elevation dimensions. A built-in material model

TABLE I : Simulation Parameters.

Parameter	Value (MMUS)	Value (SDUV)
Transducer	*xdc_focused_array*	*xdc_focused_array*
Bandwidth	60%	53%
Sampling freq.	40 MHz	40 MHz
Speed of sound	1540 m/s	1540 m/s
ARF excitation center freq.	-	4.21 MHz
ARF F/#	-	1.5
ARF focus (axial, lateral, elevation)	-	(36, 0, 0) mm
Tracking center freq.	10 MHz	6.15 MHz
Tracking Tx F/#	1.5	0.75
Tracking Rx F/#	1.5	0.75*
Tracking Tx focus (axial, lateral, elevation)	(25, 0, 0) mm	(36, 0, 0) mm
Track PRF	61.66 Hz	10 KHz
Ensemble length	300	500

* Aperture growth and dynamic Rx focusing enabled

(MAT_KELVIN-MAXWELL_VISCOELASTIC) was used to simulate a visco-elastic material with shear elasticity and shear viscosity of 6.67 kPa and 1.67 Pa.s. The duration of the ARF was 70 μs, and ARF pushes were repeated at frequency of 100 Hz. Acoustic tracking of the simulated FEM displacement was performed using Field II with 15 scatterers per resolution cell and a total of 10 independent scatter realizations following the method described in Palmeri *et. al* [19] . ARF and tracking parameters are summarized in Table 1 (3rd column). To test the effect of system SNR, white Gaussian noise was also added to each RF line in the ensemble using the *awgn* function in Matlab (Mathworks Inc, Natick MA), and displacement tracking was performed using BSS (1.5 λ mm kernel) and NCC (1.5λ kernel) methods before and after the addition of the noise. System SNRs ranging from 15-50 dB were simulated.

C. MMUS Imaging in Experimental Phantoms

Six inclusion phantoms mimicking the mechano-acoustic properties of human tissue were prepared using the procedures described in [1]. They were prepared by melting agar, in hot colloidal mixture of 0.4 mg Fe/ml SPIO (inclusion) with graphite nano powder, and congealing into cylindrical molds. The concentration of agar and graphite was 0.8%-1.5% and 3%, respectively. The volume of the inclusion was 1 cm^3.

Phantoms containing SPIO-loaded inclusions were imaged using an open-air MMUS system comprised of a UltraSonix SonixTouch with a L14-5/38 linear array transducer at 10 MHz and 2 electromagnets that provided a sinusoidally modulated magnetic gradient force at 2.0031 Hz. Data were acquired as consecutive B-Mode frames at 61.66 fps to generate 8.11s ensemble length per tracking location. Two sets of data were collected by turning on and off the magnetic field. Further detail regarding the MMUS imaging set-up can be found in [1]. Acquired RF data were transferred to a computational work station for constructing MMUS images using FPL and BSS with kernel sizes of 0.014 and 0.043 mm (Figure 1) [1]. The performance between BSS and FPL was compared using SNR, which was calculated by taking ratio of median pixel intensity inside vs outside of the inclusion (Figure 3 (b-c)).

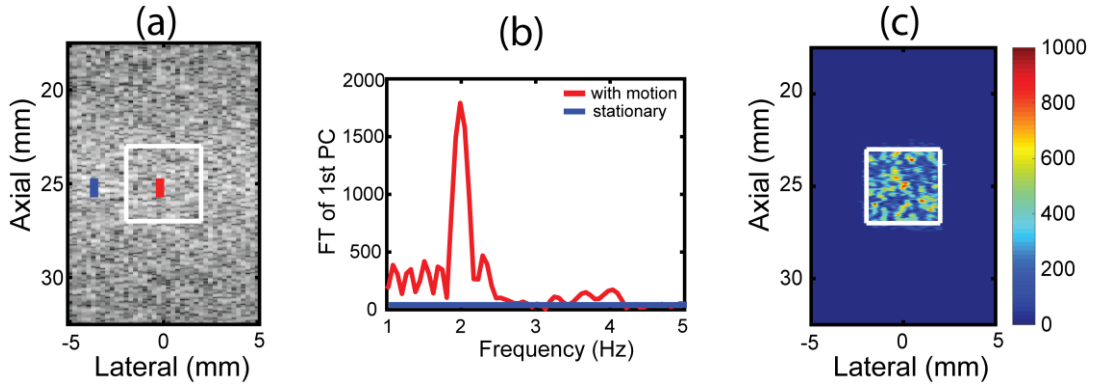

Figure 2: (a) Simulated B-mode ultrasound image with stationary (outside the white box) and non-stationary (inside the white box) scatterers. (b) Representative Fourier transforms (FT) of the phase of the 1st principal component (PC) from axial samples shown in panel (a) (red- and blue-filled rectangles). (c) Simulated parametric MMUS-type image using the BSS method. Color bar represents magnitude of the 2 Hz frequency component, as in (b).

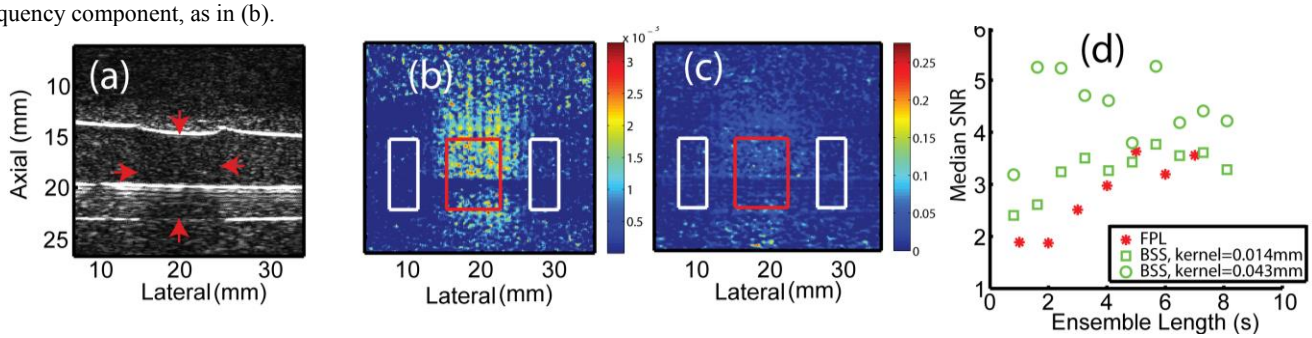

Figure 3: (a) B-mode ultrasound image of an experimental MMUS phantom. Red arrows show the boundaries of the SPIO-loaded inclusion. Parametric MMUS image using (b) BSS method with kernel length = 0.014 mm (c) FPL method after subtracting MMUS-type image constructed using 'magnetic field off' data from 'magnetic field on' data. Red and white contours denote ROI for the calculation of SNR. The ensemble length used to construct both images was 0.81s. (d) Comparison of median SNR over 6 phantoms vs ensemble length between FPL and BSS methods. Note that BSS was performed using two different kernel sizes (green square versus circle). The horizontal line in panels (a-c) near 20 mm axially is an artifact in phantom construction attributed to lack of sufficient scattering particles and/or trapped air.

D. SDUV Imaging in Calibrated Experimental Phantoms

SDUV in a CIRS 049 elasticity QA phantom (CIRS, Norfolk, VA) was performed using a Siemens Acuson Antares imaging system equipped for research purposes and a VF7-3 linear array transducer (Siemens Medical Solutions USA, Inc. Ultrasound Division). The ARF excitation was 300-cycle (70 μs) in duration and centered at 4.21 MHz with an F/1.5 focal configuration. The ARF excitation was repeated at a PRF of 100 Hz. The induced displacement was tracked by conventional two-cycle A-lines at a center frequency of 6.15 MHz and pulse repetition frequency of 11.5 kHz. The total ensemble length was 53 ms. Imaging was performed at system power level ranging from 10-55% to vary the amplitude of motion, with five repeated measures at each power level.

IV. Results and Discussion

In Figure 2(a), stationary and non-stationary scatterers are not distinguishable in the B-mode image because they have the same scattering amplitude. However, in Figure 2(b), stationary and non-stationary scatterers are differentiated by the magnitude of the 2 Hz frequency component, which is higher than for the non-stationary scatterers, as expected. Magnitude of the 2 Hz frequency component is shown parametrically in the image of Figure 2(c), which clearly delineates the non-stationary inclusion (white outline). Note that pixel intensities vary inside the inclusion because scatterers' positions and reflection coefficients varied between resolution cells. Higher reflection amplitudes from scatterers in a given resolution cell will yield higher magnitude in the corresponding reflected wave, which in turn increases the magnitude of 2 Hz component.

Figures 3(b) and (c) show parametric MMUS images using the BSS detection method and FPL method, respectively. SNR was 4.03 in the BSS-derived image and 2.2 in the FPL-generated image. The BSS, but not the FPL, method was able to contrast the inclusion even when the ensemble length was < 2 s. Median SNR across six phantoms is plotted as a function of ensemble length in panel (c) for both BSS and FPL-based detection methods. The BSS method was performed using two different kernel lengths. The larger kernel length had higher SNR but slightly blurred inclusion boundaries (data not shown for brevity). SNR was generally higher using BSS versus FPL methods, with the largest difference in SNR achieved when the ensemble length was less than 5 s.

Figure 4(a) shows the BSS- and NCC-derived viscoelastic properties from SDUV as a function of SNR for the FEM simulated data. Peak displacements ranged from 0.5 - 0.2 μm

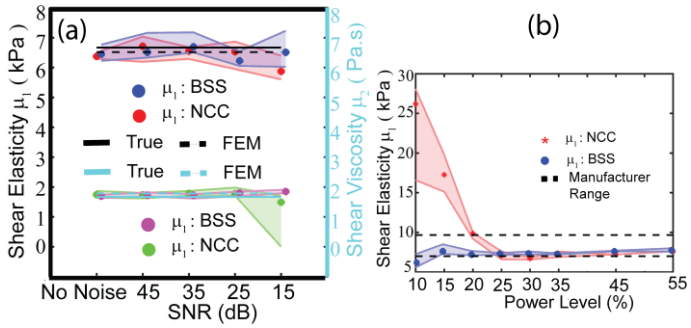

Figure 4: (a) BSS and NCC method-derived median and IQR (shaded area) of shear (μ_1) and viscous (μ_2) modulus over 10 speckle realizations with and without noise cases. Solid and dotted black lines represent true set material modulus and modulus derived using FEM displacement data, respectively. (b) BSS and NCC method-derived median and IQR (shaded area) of shear (μ_1) modulus over 5 acquisitions when power of scanner varied between 10-55%. Dotted line represents range of shear modulus of specified by the CIRS.

in the lateral locations between 0.4-2.4 mm away from the center of the ARF. The performance of BSS and NCC was comparable for SNR between 45-25dB. For SNR= 15 dB, NCC-derived coefficient of variation (100*median/IQR) of shear viscosity was 111.5 - 830% (which suggests that NCC was challenged by the low-displacement, low-SNR scenario. Figure 4(b), showing experimental phantom results, displays BSS- and NCC- derived shear elasticity as a function of scanner power level. Note that, shear viscosity is not shown because the viscosity of the CIRS elastic phantom was not specified by the manufacturers. In the CIRS elastic phantom experiment, the amplitude of the motion was $\leq$ 0.5 µm for scanner power levels $\leq$ 20%. The mean of BSS- and NCC-derived shear elasticity estimates at 55% power was considered as the validation standard for calculating percent error. The median percent error in BSS-derived shear modulus was -6.8%, -1.55%, -17.11% for power levels of 20%, 15%, and 10%, respectively. The corresponding error in NCC-derived shears elasticity estimates was 29.90%, 127.1%, 244.70%. As in the FEM simulation, NCC was unable to detect displacement < 0.5 µm in the CIRS phantom, leading to erroneous elasticity measures at the low power settings.

V. Conclusion

In this work, sub-micrometer, periodic motion detection using a BSS-based method in the context of MMUS and SDUV imaging was investigated *in silico* and experimentally. Parametric MMUS images rendered using the BSS-based method had higher SNR relative to those rendered using a FPL method even when the ensemble length was < 2 s. Future work will evaluate additional performance metrics, including contrast-to-noise ratio as a function of kernel and ensemble lengths. In SDUV imaging, the BSS-based method achieved lower error compared to the NCC method for deriving shear elasticity and viscosity in 15 dB SNR and $\leq$ 20% system power scenarios. In future work, we will compare BSS performance to Kalman filtering approaches. We will also investigate the relevance of the BSS method to detecting periodic motion in the context of Harmonic motion imaging (HMI). Overall, the results of this study suggest the relevance of using BSS for the detection of sub-micrometer, periodic motion in MMUS and SDUV imaging, particularly when SNR is less than 15 dB and/or induced displacements are less than 0.5 µm.

References

[1] A. G. Pope, *et. al*, "Contrast-enhanced imaging of SPIO-labeled platelets using magnetomotive ultrasound.," *Phys. Med. Biol.*, vol. 58, no. 20, pp. 7277–90, 2013.

[2] S. Chen, M. Fatemi, and J. F. Greenleaf, "Quantifying elasticity and viscosity from measurement of shear wave speed dispersion.," *J. Acoust. Soc. Am.*, vol. 115, no. 6, pp. 2781–5, Jun. 2004.

[3] S. Chen, *et. al*, "Shearwave dispersion ultrasound vibrometry (SDUV) for measuring tissue elasticity and viscosity.," *IEEE Trans. Ultrason. Ferroelectr. Freq. Control*, vol. 56, no. 1, pp. 55–62, Jan. 2009.

[4] E. E. Konofagou and K. Hynynen, "Localized harmonic motion imaging: Theory, simulations and experiments," *Ultrasound Med. Biol.*, vol. 29, no. 10, pp. 1405–1413, 2003.

[5] J. Vappou, C. Maleke, and E. E. Konofagou, "Quantitative viscoelastic parameters measured by harmonic motion imaging.," *Phys. Med. Biol.*, vol. 54, no. 11, pp. 3579–94, 2009.

[6] G. F. Pinton, J. J. Dahl, and G. E. Trahey, "Rapid tracking of small displacements with ultrasound.," *IEEE Trans. Ultrason. Ferroelectr. Freq. Control*, vol. 53, no. 6, pp. 1103–17, Jun. 2006.

[7] Y. Zheng, S. Chen, W. Tan, R. Kinnick, and J. F. Greenleaf, "Detection of tissue harmonic motion induced by ultrasonic radiation force using pulse-echo ultrasound and Kalman filter," *IEEE Trans. Ultrason. Ferroelectr. Freq. Control*, vol. 54, no. 2, pp. 290–299, 2007.

[8] S. a. McAleavey, K. R. Nightingale, and G. E. Trahey, "Estimates of echo correlation and measurement bias in acoustic radiation force impulse imaging," *IEEE Trans. Ultrason. Ferroelectr. Freq. Control*, vol. 50, no. 6, pp. 631–641, 2003.

[9] E. C. Elegbe and S. A. McAleavey, "Single tracking location methods suppress speckle noise in shear wave velocity estimation.," *Ultrason. Imaging*, vol. 35, no. 2, pp. 109–25, Apr. 2013.

[10] W. F. Walker and G. E. Trahey, "A Fundamental Limit on Delay Estimation Using Partially Correlated Speckle Signals," *IEEE Trans. Ultrason. Ferroelectr. Freq. Control*, vol. 42, no. 2, pp. 301–308, 1995.

[11] A. P. Kadi and T. Loupas, "On the performance of regression and step-initialized IIR clutter filters for color Doppler systems in diagnostic medical ultrasound," *IEEE Trans. Ultrason. Ferroelectr. Freq. Control*, vol. 42, no. 5, pp. 927–937, Sep. 1995.

[12] C. M. Gallippi, K. R. Nightingale, and G. E. Trahey, "BSS-based filtering of physiological and ARFI-induced tissue and blood motion," *Ultrasound Med. Biol.*, vol. 29, no. 11, pp. 1583–1592, 2003.

[13] C. M. Gallippi and G. E. Trahey, "Adaptive Clutter Filtering via Blind Source Separation for Lateral Blood Velocity Measurement," *Ultrason. Imaging*, vol. 24, no. 2002, pp. 193–214, 2002.

[14] F. W. Mauldin, H. T. Zhu, R. H. Behler, T. C. Nichols, and C. M. Gallippi, "ROBUST PRINCIPAL COMPONENT ANALYSIS AND CLUSTERING METHODS FOR AUTOMATED CLASSIFICATION OF TISSUE RESPONSE TO ARFI EXCITATION."

[15] F. W. Mauldin, F. Viola, and W. F. Walker, "Complex principal components for robust motion estimation.," *IEEE Trans. Ultrason. Ferroelectr. Freq. Control*, vol. 57, no. 11, pp. 2437–49, Nov. 2010.

[16] J. V. Stone, "Independent component analysis: an introduction," *Trends Cogn. Sci.*, vol. 6, no. 2, pp. 59–64, 2002.

[17] A. Jensen, "Calculation of Pressure Fields from Arbitrarily," *IEEE Trans. Ultrason. Ferroelectr. Freq. Control*, vol. 39, no. 2, pp. 262–267, 1992.

[18] J. A. Jensen, D.- Lyngby, P. Medical, B. Engineering, and I. Technology, "Field : A Program for Simulating Ultrasound Systems Field : A Program for Simulating Ultrasound Systems," *10th Nord. Conf. Biomed. Imaging*, vol. 34, pp. 351–353, 1996.

[19] M. L. Palmeri, *et. al* "A finite-element method model of soft tissue response to impulsive acoustic radiation force.," *IEEE Trans. Ultrason. Ferroelectr. Freq. Control*, vol. 52, no. 10, pp. 1699–712, Oct. 2005.